

Reduced Charge Diffusion in Thick, Fully Depleted CCDs With Enhanced Red Sensitivity

Jessamyn A. Fairfield, Donald E. Groom, Stephen J. Bailey, Christopher J. Bebek, *Member, IEEE*, Stephen E. Holland, *Member, IEEE*, Armin Karcher, William F. Koble, Wolfgang Lorenzon, and Natalie A. Roe

Abstract—Lateral charge diffusion in charge-coupled devices (CCDs) dominates the device point-spread function (PSF), which can affect both image quality and spectroscopic resolution. We present new data and theoretical interpretations for lateral charge diffusion in thick, fully depleted CCDs developed at Lawrence Berkeley National Laboratory (LBNL). Because they can be overdepleted, the LBNL devices have no field-free region and diffusion is controlled through the application of an external bias voltage. Recent improvements in CCD design at LBNL allow the application of bias voltages exceeding 200 V. We give results for a 3512×3512 format, $10.5 \mu\text{m}$ pixel back-illuminated p-channel CCD developed for the SuperNova/Acceleration Probe (SNAP), a proposed satellite-based experiment designed to study dark energy. Lateral charge diffusion, which is well described by a symmetric two-dimensional (2-D) Gaussian function, was measured at substrate bias voltages between 3 and 115 V. At a bias voltage of 115 V, we measure a root-mean square (rms) diffusion of $3.7 \pm 0.2 \mu\text{m}$. Lateral charge diffusion in LBNL CCDs will meet the SNAP requirements.

Index Terms—Charge-coupled device (CCD), diffusion processes, high-resistivity silicon, optical transfer functions.

I. INTRODUCTION

LATERAL charge diffusion occurs during the movement of photo-generated carriers in a charge-coupled device (CCD) as they travel from the point of generation to the potential wells where the charge is collected. Pixel size and lateral charge diffusion are the primary factors determining the spatial resolution of a CCD. In thin back-illuminated CCDs used for astronomical imaging, the lateral diffusion is approximately equal to the thickness of the field-free region, typically on the order of $5\text{--}10 \mu\text{m}$. By contrast, the LBNL thick, fully depleted CCDs [1] have no field-free region, and charge created near the backside must drift across the thick substrate ($200\text{--}300 \mu\text{m}$) to reach the pixel. Although the lateral charge diffusion increases linearly with the device thickness, with sufficient overdepletion of the substrate it can be reduced below the values typical in thin devices.

The thick substrate enhances the efficiency for detection of long-wavelength photons, increasing the quantum efficiency (QE) in the near-infrared (NIR), and minimizing fringing [2].

Manuscript received March 29, 2006; revised July 6, 2006. This work was supported by the U.S. Department of Energy under Contract DE-AC03-76SF0098.

J. A. Fairfield, D. E. Groom, S. J. Bailey, C. J. Bebek, S. E. Holland, A. Karcher, W. F. Koble, and N. A. Roe are with the Lawrence Berkeley National Laboratory, Berkeley, CA 94720 USA (e-mail: NARoe@lbl.gov).

W. Lorenzon is with the University of Michigan, Ann Arbor, MI 48109 USA. Color versions of one or more of the figures in this paper are available online at <http://ieeexplore.ieee.org>.

Digital Object Identifier 10.1109/TNS.2006.885793

Since both the lateral charge diffusion and the QE increase linearly with substrate thickness, the device thickness must be optimized to trade off red QE with lateral charge diffusion. Reduction of diffusion through application of a large substrate bias voltage facilitates the achievement of high NIR QE without sacrificing good spatial resolution.

The LBNL devices are fabricated from high-resistivity ($4\text{--}10 \text{ k}\Omega/\text{cm}$), weakly doped, n-type silicon, with p-type channels made with boron implants. The charge carriers collected are holes. This design was chosen as a result of the straightforward implementation of extrinsic gettering techniques for low dark current with n-type high-resistivity silicon and for increased radiation hardness [3]. The substrate can be fully depleted with a bias voltage, typically in the range of $15\text{--}30 \text{ V}$ for a $200 \mu\text{m}$ thick CCD. Overdepletion of the substrate reduces lateral diffusion since the charge transport velocity increases with large electric fields. Recent design changes have produced devices that can operate at substrate voltages exceeding 200 V [4].

The LBNL CCDs are well suited for space and ground-based astronomical imaging and spectroscopy. The devices tested here were developed specifically for a large pixel-count focal plane in SNAP [5], a proposed satellite experiment designed to observe approximately 2000 high-redshift supernovas and carry out a weak-lensing survey to study dark energy. For good quantum efficiency in the NIR, the SNAP CCDs will have a substrate thickness of $200 \mu\text{m}$, while to achieve the good spatial resolution required for weak lensing, the rms charge diffusion should be comparable to the effects of diffraction and thus should not exceed $4 \mu\text{m}$ [6], [7]. We describe here the characterization of lateral charge diffusion in the thick, high-voltage SNAP CCDs as a function of the applied bias voltage using a previously reported technique [8].

II. MEASUREMENT PRINCIPLE

The virtual knife edge method, originally developed in [8], is based on the Foucault knife-edge technique, which is used to determine the profile of a light beam. An obstructing device is placed at the focus of a pinhole projector. The projected beam is scanned across the object edge. Data for intensity versus beam position, assuming a Gaussian beam profile, can be fitted to an error function to extract the beam width.

The idea behind a virtual knife edge experiment is similar. Instead of a physical obstruction blocking the light, a region of pixels over which the signal from the spot is summed is used, and this region is referred to as the integration area. A set of images with varying integrated intensities is acquired as the spot is moved out of the integration area. The edge of the integration area serves the same function as the physical knife edge. Fig. 1 is

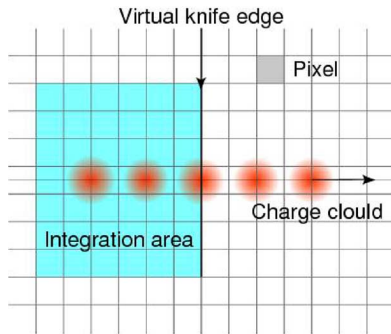


Fig. 1. The virtual knife edge concept. The spot is scanned to the right over the pixels on the CCD and eventually exits the integration area. The summed charge in the integration area exhibits an error function shape.

an illustration of the concept. The technique has the advantage of being independent of the physical pixel size and having no scattered light from a physical knife edge.

A plot of the total light in the integration area for each image scan position follows an error function with a transition width determined by the convolution of the beam width and the lateral charge diffusion. Fitting the scan data with an error function, or equivalently fitting its derivative with a Gaussian, yields a measurement of the lateral charge diffusion of the CCD.

III. EXPERIMENTAL APPARATUS

The general procedure begins by cooling the CCD to 133 K inside a liquid-nitrogen dewar operated at 10^{-5} torr. We use an autotuning temperature controller to maintain the temperature to within 0.1 K. The front of the dewar has an antireflection coated glass window and faces into a light-tight box. A shutter is used to control exposure times. An Oriel monochromator driven by a xenon arc lamp provides 550 nm light via an optical fiber to a 10 μm pinhole followed by a 25-mm-long collimator. Scattered light is reduced by a blackened, threaded baffle on the inside of the tube. The collimated pinhole is focused on the CCD by a Mitutoyo 34-mm working-distance microscope objective. The theoretically achievable full width at half maximum (FWHM) of the focused light beam is 2.6 μm at 550 nm. The projector sits inside the light-tight box on an x - y - z translation stage. The motor stage is carefully aligned so that the x -axis is parallel to the CCD rows and the z -axis is parallel to the columns. Both axes are coplanar with the CCD surface.

The CCD is controlled and read out by a modified Astronomical Research Cameras Gen II controller.¹ The utility board is configured to control the exposure timing, shutter operation, x - y - z motion of the projector, and position encoder readout. Java-based software manages the controller for data acquisition, and the data are analyzed using tools developed in Research Systems, Inc. IDL.

IV. EXPERIMENTAL PROCEDURE

A. Preliminary Measurements

The Foucault knife-edge technique, using a razor blade, was used to measure the beam size. The measured rms width was 1.2

$\pm 0.1 \mu\text{m}$, which is consistent with the theoretical expectation. To focus the spot on the CCD, we start with a substrate voltage of 55 V, which is sufficient to overdeplete the CCD. We first center the spot on one pixel. We then adjust the distance from the projector to the CCD using the motorized focus stage and compare the signal in the nearest-neighbor pixels to the central pixel. When the ratio of the two is minimized, the spot is focused. The distance between the projector and the CCD could be maintained with a precision of 20 μm for up to eight hours.

We used the ratio of nearest neighbors to the central pixel to test whether the focused spot remained on-axis after significant lateral translation by scanning multiple times in all directions and noting the drift. We found an average offset in the x -direction of 0.40 μm per 100 μm of motion in the z -direction, and 0.76 μm of drift in the z -direction per 100 μm of motion in the x -direction. In a normal scan, covering 200 μm along the x -axis, the offset was less than 0.5%, which is not significant.

Pixel-to-pixel nonuniformity can complicate the lateral diffusion measurements. Because of variations in the fabrication process, different pixels may have slightly different light response. To determine the degree to which this would affect our data, we scanned the spot across several pixels and then plotted the pixel response. We found that the pixel response was uniform to within 2%, therefore, no correction was necessary.

B. Diffusion Measurement

Our scans varied in substrate voltage from 3 to 115 V and each had 150 images on average. The scans covered 10–60 pixels with step size from 0.4–40 μm . We varied the step size as a function of voltage since, at low voltages, diffusion is large and large step sizes more efficiently spanned the pixels containing the charge. The size of the integration area was also varied with substrate voltage. A square of about five times the rms diffusion on each side was used for the integration area; larger integration squares introduced additional read noise and degraded the fit error, while smaller integration squares did not completely contain the generated charge. Fig. 2 shows the collected charge distribution in an array of CCD pixels at several voltages, demonstrating the variation of diffusion with voltage.

To optimize the signal-to-noise ratio, we adjusted the exposure time to have as many photons as possible without saturating the pixels. Exposure times varied from 0.1–10 s, and were selected to fill the pixel wells one-third full. At low voltages, longer exposure times were required since charge diffused into more neighboring pixels. At high voltages, we were careful to keep the exposure time short enough to avoid saturating the central pixel and blooming into neighboring pixels.

During data taking we monitored the baseline level of the CCD. We repeated measurements for any scan point that exhibited abnormal fluctuations due to excess background noise. We also scanned over the same set of pixels each time to avoid any pixel-to-pixel variation. All of the scans were taken across the channel stops (along the row direction), as previous work showed no difference between diffusion measured in the row and column directions [8]. All data were taken with 550 nm light, which is absorbed within a few μm of the surface [2]. Previous studies observed no difference in the lateral charge diffusion as a function of wavelength from 450 to 650 nm [8]. The

¹Astronomical Research Cameras, Inc., 3547 Camino del Rio South, San Diego, CA 92108; e-mail leach@mintaka.sdsu.edu.

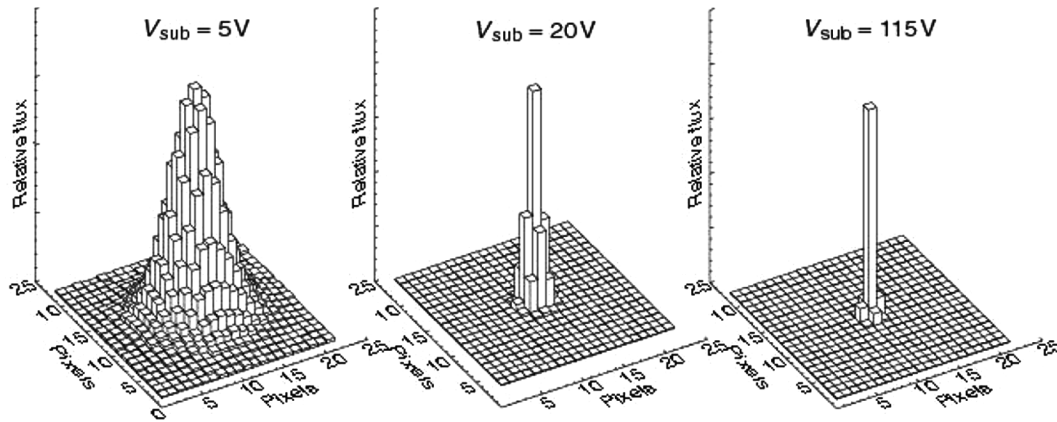


Fig. 2. The CCD response profile to a $1.2\text{-}\mu\text{m}$ rms beam spot for three different substrate bias voltages. Full depletion is reached at 20 V. Each grid box is a $10.5\text{-}\mu\text{m}$ pixel and the height is the detected charge, with arbitrary normalization that varies between plots.

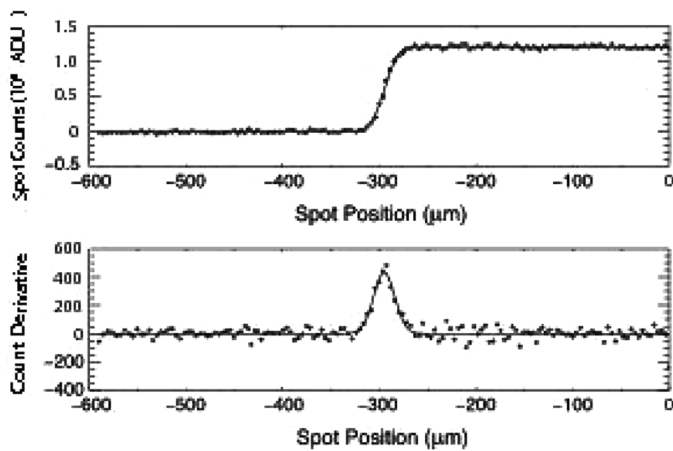


Fig. 3. Sample scan analysis of a SNAP CCD. Top: the measured CCD counts in the integration area versus the beam position, fit to an error function. Bottom: the derivative of the top, fit with a Gaussian. The two fits are compared as a consistency check, yielding an error function sigma of $10.8 \pm 0.002\text{-}\mu\text{m}$ and a Gaussian sigma of $10.9 \pm 0.6\text{-}\mu\text{m}$.

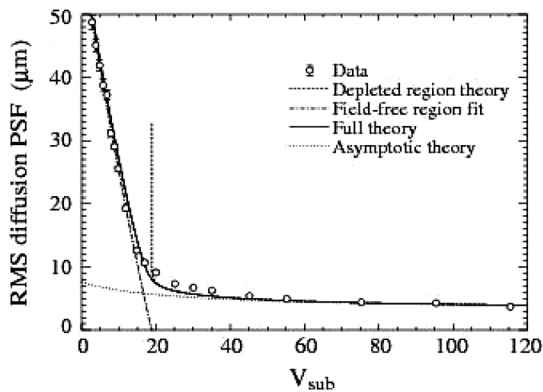


Fig. 4. The measured rms diffusion PSF (data points) as a function of the substrate bias voltage. The data are for a $193\text{-}\mu\text{m}$ thick SNAP CCD, and at the highest voltage, the diffusion is lower than the $4\text{-}\mu\text{m}$ SNAP design goal. The field-free region line is the theoretical fit for operation below full depletion, the depleted region line is the theoretical prediction for overdepleted operation, and the asymptotic theory line is the simplified limit of the depleted region theory. The full theory line is the convolution of the field-free and depleted theories.

photon absorption length grows with increasing wavelength and decreasing temperature, reaching $\sim 60\text{-}\mu\text{m}$ at 900 nm and 133 K

TABLE I
RMS DIFFUSION MEASUREMENTS ARE TABULATED VERSUS SUBSTRATE BIAS VOLTAGE. THE BEAM SPOT SIZE HAS BEEN SUBTRACTED IN QUADRATURE. THE ERRORS ARE STATISTICAL ONLY

V_{sub} (V)	Diffusion (μm)	Error (μm)
2.84	48.8	1.1
3.82	45.1	1.0
4.83	41.9	0.9
5.83	38.8	0.9
6.84	37.3	0.8
7.87	31.1	0.6
8.89	29.1	0.4
9.86	25.6	0.4
11.91	19.3	0.4
14.90	12.6	0.3
16.96	10.7	0.3
19.94	9.1	0.3
25.10	7.3	0.2
30.10	6.7	0.2
35.04	6.3	0.3
45.20	5.4	0.3
55.20	4.9	0.3
75.30	4.4	0.2
95.40	4.3	0.2
115.40	3.7	0.2

[2]. This might be expected to result in a reduction of lateral charge diffusion at NIR wavelengths, if the spot focus does not rapidly diverge with depth or grow due to diffraction.

Once the setup was completed and the spot size was characterized, we collected data with a $15\text{-}\mu\text{m}$ pixel CCD similar to the one previously characterized [8]. We found that we were able to reproduce the previous results. We then moved on to the high-voltage SNAP CCD, a 3512×3512 , $193\text{-}\mu\text{m}$ -thick, $10.5\text{-}\mu\text{m}$ pixel, back-illuminated device. Fig. 3 shows typical data from one scan of the SNAP CCD and its derivative. Also shown are fits to an error function and a Gaussian, respectively. The Gaussian-fit rms diffusion, with the beam spot size subtracted in quadrature, is plotted as a function of substrate voltage in Fig. 4 and tabulated in Table I.

C. Systematic and Statistical Errors

Once we had taken scans, we checked the robustness of the data in several ways. We compared error function and Gaussian

fits. The diffusion results were in good agreement, but the Gaussian method was found to be less sensitive to fluctuations at the end points of the scan. We also collected data for several sizes of integration areas and several positions of the virtual knife edge in the software. Similar results were obtained within the statistical errors.

We investigated statistical uncertainties due to shot noise and read noise. The read noise was ~ 20 analog-to-digital units (ADUs), small compared to the shot noise on the signal, which varied from 300–750 ADUs (2%–5%) for most substrate voltages. The measurement error was dominated by the statistical uncertainties on the data points due to shot noise; therefore, we took a large number of diffusion data points in order to mitigate this.

There can be systematic errors, discussed above, due to pixel-to-pixel nonuniformity and focus precision. The pixel-to-pixel uniformity error was found to be small. The focus drifted by small amounts, but not significantly during scans.

V. THEORY

We first review the original theory initially developed in [9], and then describe modifications required to fit the data accurately. The distribution of charges is Gaussian, with a distribution determined by the electric field shape, the diffusion coefficient and the transit time. If the CCD is not fully depleted, diffusion is dominated by the field-free region; the field is zero in the field-free region and increases linearly to E_{\max} , the electric field at the junction between the buried channel and the substrate. If the CCD is overdepleted, the field increases linearly from E_D at the backside ohmic contact to E_{\max} . We consider these two cases separately.

A. Diffusion in an Overdepleted CCD

The charge drift velocity v_d is proportional to E at low E : $v_d = \mu E$ where μ is the carrier mobility. We can integrate this equation [9], to find the overdepleted diffusion variance

$$\sigma_{\text{od}}^2 = \frac{2k_B T}{q} \frac{\epsilon_{\text{Si}}}{qN_D} \ln \left(\frac{E_{\max}}{E_{\min}} \right) \quad (1)$$

where we have used the Einstein relationship $D/\mu = k_B T/q$. D is the diffusion coefficient, k_B is the Boltzmann constant, T is the temperature in kelvins, q is the electron (or hole) charge, ϵ_{Si} is the permittivity of silicon, and N_D is the dopant density. For high constant fields, i.e., neglecting space charge in the depleted region, the asymptotic form of (1) is

$$\sigma_{\text{asympt}}^2 = 2 \frac{k_B T}{q} \frac{y_D^2}{V_{\text{sub}} - V_{J'}} \quad (2)$$

where y_D is the device thickness, V_{sub} is the substrate voltage, and $V_{J'}$ is the effective junction potential [1]. For high substrate voltages, above 50 V, we can use the asymptotic form to predict the diffusion.

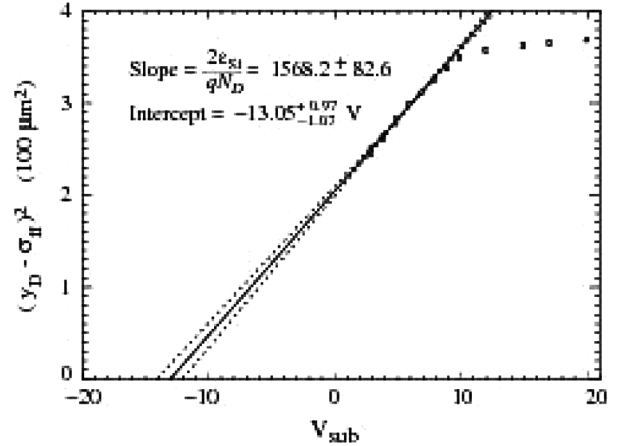


Fig. 5. The low-voltage linear fit used to determine parameters for the high-voltage fit. Here the square of the wafer thickness minus diffusion is plotted against the substrate voltage. The V_{sub} intercept is the junction voltage and the slope contains the carrier density.

B. Diffusion in a CCD With a Field-Free Region

In the case of a CCD that is not fully depleted, diffusion in the field-free region dominates. In this case, the total rms width is approximately equal to the thickness of the field-free region [10]. We can write this as the device thickness minus the thickness of the depleted region

$$\sigma_{\text{ff}} = y_D - \sqrt{\frac{2\epsilon_{\text{Si}}}{qN_D} (V_{\text{sub}} - V_{J'})}. \quad (3)$$

In the region where the diffusion contributions from the field-free and depleted regions are comparable, we use an interpolation algorithm developed in [10] to predict the diffusion.

C. Comparing Data to Theory

In order to compare our data to theory, we first used (3) to fit the quantity $(y_D - \sigma_{\text{ff}})^2$, which is linear at low voltages. We extracted a depletion voltage of 18.1 V, a dopant density $N_D = 1.2 \times 10^{12} \text{ cm}^{-3}$, and a junction voltage $V_{J'} = -17.1$ V. The fit is shown in Fig. 5. With these parameters we calculate the overdepleted diffusion given by (1). At voltages well above the depletion voltage, our data were consistently 30%–40% above the theoretical predictions. After repeated checks of the apparatus, beam size, and fit calculations, we remained convinced of the accuracy of our experimental data.

D. New Developments in the Theory

We believe the discrepancy between the data and the asymptotic theory lies in a reduction of carrier mobility with increasing electric field. At low electric fields, charge velocity and charge transit time depend linearly on field strength. As field strength increases, the velocity field-dependence becomes nonlinear as the scattering of energetic charge carriers increases, primarily

due to optical phonon emission [11]. This effect can be expressed as a correction to the carrier mobility [12]. The mobility is modified such that

$$\mu(T, E) = \frac{\mu_0(T)}{m(T, E)} \quad (4)$$

where $\mu_0(T) = 1.31 \times 10^8 T^{-2.20} \text{ cm}^2/\text{V}\cdot\text{s}$ is the low-field mobility for holes and $m(T, E)$ is a correction factor given by

$$m(T, E) \approx [1 + (E/E_c)^\beta]^{1/\beta} \quad (5)$$

where the critical field $E_c = 1.24T^{1.68} \text{ V/cm}$ and $\beta = 0.46T^{0.17}$ [13]. The drift velocity can now be written using the modified mobility

$$v_d(T, E) = \mu(T, E)E. \quad (6)$$

For high fields, we can replace E by its average value $\langle E \rangle$ and calculate the transit time, t_{tr} , for a device of thickness y_D

$$t_{\text{tr}} = \frac{y_D}{v_d} = \frac{y_D}{\mu(T, E)E} \quad (7)$$

$$= \frac{y_D^2}{\mu(T, E)(V_{\text{sub}} - V_J)}. \quad (8)$$

Using this high-field transit time to find the asymptotic diffusion yields

$$\sigma_{\text{asympt}}^2 = 2Dt_{\text{tr}} = 2 \frac{D}{\mu(T, \langle E \rangle)} \frac{y_D^2}{(V_{\text{sub}} - V_J)}. \quad (9)$$

Using Einstein's equation again, the resulting expression for the asymptotic lateral charge diffusion is

$$\sigma_{\text{asympt}}^2 = 2 \frac{k_B T}{q} \frac{y_D^2}{(V_{\text{sub}} - V_J)} m(T, \langle E \rangle). \quad (10)$$

The revised theoretical predictions are plotted in Fig. 4. The asymptotic form is a better fit to the data at voltages significantly above the depletion voltage. Overall, the inclusion of the field dependence of mobility yields excellent agreement between data and theory at high voltage. There is still a small disparity near the depletion voltage, where the data are higher than the improved theoretical predictions. It is possible that there are additional temperature and field dependences in the diffusion coefficient [14]–[16].

VI. CONCLUSION

We created a stable experimental setup that allowed for the measurement of lateral charge diffusion in CCDs. We measured lateral charge diffusion in thick, fully depleted CCDs. The voltage dependence of the experimental data motivated a modification of the theory to correctly account for high field effects. At a substrate voltage of 115 V, we measured an rms lateral charge diffusion of $3.71 \pm 0.16 \mu\text{m}$, which meets the SNAP requirements. Future work will include intrapixel response studies, measurements of effects at the edge pixels of the CCD and investigation of lateral charge diffusion at near infrared wavelengths.

REFERENCES

- [1] S. E. Holland, D. E. Groom, N. P. Palaio, R. J. Stover, and M. Wei, "Fully-depleted, back-illuminated charge-coupled devices fabricated on high-resistivity silicon," *IEEE Trans. Electron Devices*, vol. 50, no. 3, 2003.
- [2] D. E. Groom, S. E. Holland, M. E. Levi, N. P. Palaio, S. Perlmutter, R. J. Stover, and M. Wei, "Quantum efficiency of a back-illuminated CCD imager: An optical approach," *SPIE*, vol. 3649, pp. 80–90, 1999.
- [3] C. J. Bebek, "Proton radiation damage in p-channel CCDs fabricated on high-resistivity silicon," *IEEE Trans. Nucl. Sci.*, vol. 49, pp. 1221–1225, 2002.
- [4] W. F. Kolbe, S. E. Holland, and C. J. Bebek, "CCD development progress at Lawrence Berkeley National Laboratory," in *Proc. Scientif. Detect. Wkshp. 2005*, Taormina, Italy.
- [5] G. Aldering, "Overview of the supernova/acceleration probe (SNAP)," in *Proc. SPIE*, 2002, vol. 4835, pp. 146–157.
- [6] J. Rhodes, "Weak lensing from space I: Instrumentation and survey strategy," *Astropart. Phys.*, vol. 20, pp. 377–389, 2004.
- [7] M. Lampton, "SNAP telescope: An update," in *Proc. SPIE*, vol. 5166, pp. 113–123.
- [8] A. Karcher, "Measurement of Lateral charge diffusion in thick, fully depleted, back-illuminated CCDs," *IEEE Trans. Nucl. Sci.*, vol. 51, no. 5, pp. 2231–2237, 2004.
- [9] S. E. Holland, "Development of back-illuminated, fully-depleted CCD image sensors for use in astronomy and astrophysics," in *Proc. IEEE Workshop on Charge-Coupled Devices and Adv. Image Sens.*, Bruges, Belgium, 1997, pp. R26-1–R26-4.
- [10] D. Groom, "Point-spread function in depleted and partially depleted CCDs," in *Proc. 4th ESO Workshop on Opt. Detect. Astron.*, 1999, pp. 205–216.
- [11] S. M. Sze, *Physics of Semiconductor Devices*. New York: Wiley, 1981, ch. 1.
- [12] C. Jacoboni, C. Canali, G. Ottaviani, and A. Quaranta, "A review of some charge transport properties of silicon," *Solid State Electron.*, vol. 20, pp. 77–89, 1977.
- [13] C. Canali, G. Majni, R. Minder, and G. Ottaviani, "Electron and hole drift velocity measurements in silicon and their empirical relation to electric field and temperature," *IEEE Trans. Electron Dev.*, vol. 22, pp. 1045–1046, 1975.
- [14] D. J. Bartelink and G. Persky, "Diffusion of electrons in silicon transverse to a high electric field," *Appl. Phys. Lett.*, vol. 16, no. 5, pp. 191–194, 1970.
- [15] L. Reggiani, R. Brunetti, and E. Normantas, "Diffusion coefficient of holes in silicon by Monte Carlo simulation," *J. Appl. Phys.*, vol. 59, no. 4, pp. 1212–1215, 1986.
- [16] J. M. Hinckley and J. Singh, "Anisotropic high-field diffusion of holes in silicon," *Appl. Phys. Lett.*, vol. 66, no. 20, pp. 2727–2729, 1995.